

***RHIZOPHORA* SPP. AND EPOXY RESIN BASED
SEMI-ANTHROPOMORPHIC LIVER
PHANTOM FOR LESIONS ENHANCEMENT IN
COMPUTED TOMOGRAPHY**

MARWAN AHMED MOSTAFA AL-SHIPLI

UNIVERSITI SAINS MALAYSIA

2019

***RHIZOPHORA* SPP. AND EPOXY RESIN
BASED SEMI-ANTHROPOMORPHIC LIVER
PHANTOM FOR LESIONS ENHANCEMENT IN
COMPUTED TOMOGRAPHY**

by

MARWAN AHMED MOSTAFA AL-SHIPLI

**Thesis submitted in fulfilment of the requirements
for the degree of
Doctor of Philosophy**

March 2019

ACKNOWLEDGEMENT

The submission of this thesis gives me the best opportunity to express all praise and thanks to Allah, the Almighty, the Most Merciful, the Most Passionate for granting me the strength to complete this work. This thesis would not have been possible without the guidance and help of several individuals, who in one way or another contributed to and provided me with their valuable assistance in the preparation and completion of this study. It is a great pleasure to convey my warmest gratitude and deepest appreciation to all of the min these lines of my humble acknowledgment.

I would like to thank my main supervisor Dr. Norlaili Ahmad Kabir from the bottom of my heart for her great support and continuous guidance throughout my Ph.D. research work. She has had the patience to go through the thesis, edit, and correct my write-up. I attribute the level of my Ph.D. degree to her great help and encouragement. One simply could not wish for a better or friendlier supervisor.

I would also like to express my great thanks to my co-supervisor, Prof. Dr. Rokiah Hashim for her supervision, advice, and guidance from the very early stages of this study. She provided me with extraordinary experience throughout my Ph.D. study. To her, I am eternally grateful. I extend my deepest regards to Prof. Dato' Dr. Abd Aziz bin Tajuddin who has contributed in co-supervising my Ph.D. research. His guidance, insightful comments, and suggestions have indeed helped me during the stages of writing this thesis.

Special thanks go to the supporting staff of the laboratories in the School of Physics, the School of Industrial Technology, and the Advanced Medical and Dental Institute (AMDI), who helped me in many ways to conduct the experiments in a specific manner. I also would like to acknowledge the staff at the Medical Radiology Department, CT Scan Unit, Institut Perubatan dan Pergigian Termaju for help and guidance throughout my Ph.D. research work.

My gratitude and acknowledgment are extended to those, who helped and contributed to this study through their great ideas and ample advice, especially Dr. Mohammed Wasef, Dr. Emad Ayasrh, Dr. Putri Leja, Dr. Ammar Oqlat, Dr. Mohammed Fahmi, Dr. Enas Majed, Mrs. Suzana Mat Isa, Mr. Basrul and Mr. Mohd Rizal Mohd Rodin. Without them, this study would not be possible.

To my soul, to my everything in this life, my beloved father (May Allah grant eternal peace and blessings to his soul) and my mother, I dedicate this humble work to you. To my brothers and sisters, you are the apple of my eye. Thank you so much for being part of my life. Special thanks go to my uncles, as well as all my family members for their trust in me. I am profoundly grateful to them.

Finally, I extend my deepest regards and blessings to all those, who supported me in any aspect during the completion of this research. I apologize that I could not mention them all.

TABLE OF CONTENTS

ACKNOWLEDGEMENT	ii
TABLE OF CONTENTS	iv
LIST OF TABLES	vii
LIST OF FIGURES	x
LIST OF ABBREVIATIONS	xvii
ABSTRAK	xix
ABSTRACT	xxi
CHAPTER 1 - INTRODUCTION	
1.1 Introduction	1
1.2 Problem Statement	6
1.3 Research Objectives	8
1.4 Scope of the Study.....	9
1.5 Structure of the Thesis.....	10
CHAPTER 2 - THEORY AND LITERATURE REVIEW	
2.1 The Liver	11
2.1.1 Liver Lesions	13
2.2 Medical Physics Phantoms.....	23
2.2.1 <i>Rhizophora</i> spp.	26
2.2.2 Epoxy Resin.....	31
2.2.3 Using Currently Available CT Liver Phantoms in Liver Lesion Diagnosis	34
2.3 CT Image Enhancement using Histogram Equalization Techniques.....	43
2.3.1 Contrast Stretching	46
2.3.2 Contrast Limited Adaptive Histogram Equalization (CLAHE)	48

CHAPTER 3 - MATERIALS, INSTRUMENTS AND METHODOLOGY

3.1	Materials.....	53
3.1.1	Phantom Materials	53
3.2	Instruments	57
3.2.1	Characterization Equipments	57
3.2.2	Attenuation Measurements	62
3.2.3	SAL Phantom Scanning.....	64
3.3	Methodology	67
3.3.1	Phantom Design.....	67
3.3.2	Evaluating the Effects of Adding Epoxy Resin to <i>Rhizophora</i> spp. Particleboards.....	78
3.3.3	Physical and Radiological Properties of SAL Phantom Materials.....	84
3.3.4	SECT and DECT Scanning Parameters.....	89
3.3.5	Image Quality and Analysis.....	92
3.3.6	Image Processing Methods	98
3.3.7	Image Quantitive Study via Statistical Analysis.....	103

CHAPTER 4 - RESULTS AND DISCUSSION

4.1	SAL Phantom	105
4.1.1	The Effects of Adding Epoxy Resin to <i>Rhizophora</i> spp. Particleboards..	106
4.1.2	Physical and Radiological Properties of SAL Phantom Materials.....	117
4.2	Image Quality and Analysis	134
4.2.1	Contrast and Contrast Noise Ratio Measurements for Original SAL Images	134

4.2.2 Contrast and Contrast Noise Ratio Measurements for Post-Processing
SAL Images140

4.2.3 The Optimum Protocol to Enhance the Visibility of Liver Lesions.....150

CHAPTER 5 -CONCLUSION AND RECOMMENDATIONS

5.1 Conclusions155

5.2 Limitations and Recommendations of the Study158

REFERENCES.....159

APPENDICES

LIST OF PUBLICATION

LIST OF TABLES

		Page
Table 2.1	Dimensions of adult human liver	12
Table 2.2	Summary of the literature about tube voltage (kVp) settings capability in assessing the conspicuity of different types of liver lesions	17
Table 2.3	Elemental compositions, mass density, and effective atomic number (Z_{eff}) of the body soft tissues (brain, kidney, and liver tissues) and common water-equivalent phantom materials (McCullough, 1975; Watanabe & Constantinou, 2006)	25
Table 2.4	Overview on the previous work done in the study of <i>Rhizophora</i> spp. wood and <i>Rhizophora</i> spp. particleboards as phantom materials	30
Table 3.1	Main physical and chemical properties of the Americium-241 (^{241}Am) and Cadmium-109 (^{109}Cd) gamma sources	64
Table 3.2	Characteristics of Catphan 600 phantom modules	67
Table 3.3	Main scanning parameters of SECT and DECT liver protocols. Further details can be referred in Table F.1- F.5 of Appendix F.	91
Table 4.1	The average modulus of rupture (MOR), internal bond (IB) strength, thickness swelling (TS), and water absorption (WA) of epoxy resin– <i>Rhizophora</i> spp. particleboards at different epoxy resin percentages of 0%, 5%, 10%, and 15%	109
Table 4.2	Full-Width at Half-Maximum (FWHM) and crystallinity index measurements of <i>Rhizophora</i> spp. particleboards bonded with epoxy resin at levels of 0%, 5%, 10%, and 15%	115
Table 4.3	Chemical functional groups in FTIR spectra of the <i>Rhizophora</i> spp. particleboards bonded with epoxy resin at levels of 0%, 5%, 10%, and 15 %	117
Table 4.4	Average mass density of epoxy resin with <i>Rhizophora</i> spp. particleboards at different epoxy weight percentages (0, 5, 10, and 15%), epoxy resin, and epoxy resin mixed with CaCO_3 (Further calculations can be referred in Appendix B)	119

Table 4.5	Elemental composition and effective atomic number values of epoxy resin– <i>Rhizophora</i> spp. particleboards fabricated at various epoxy resin percentages (0%, 5%, 10%, and 15%), epoxy resin, and water (Further calculations can be referred in Appendix C)	121
Table 4.6	The density, linear attenuation (μ) (cm^{-1}) and mass attenuation (μ/ρ) (cm^2/g) coefficients of epoxy resin and <i>Rhizophora</i> spp. particleboards bonded with 5%, 10%, and 15% epoxy resin at the photon energy of 26.3, 59.5 and 88.0 keV	125
Table 4.7	Relative difference values of the linear attenuation coefficients (μ) at 26.3, 59.5 and 88 keV photon energies of <i>Rhizophora</i> spp. particleboards bonded with 5%, 10%, and 15% epoxy resin compared with the calculated value of water XCOM	125
Table 4.8	The χ^2 value of the mass attenuation coefficient of <i>Rhizophora</i> spp. particleboards bonded with (5%, 10%, and 15%) epoxy resin to water (XCOM)	125
Table 4.9	Relative difference values of the linear attenuation coefficients (μ) at 26.3, 59.5, and 88 keV photon energies for the epoxy resin sample, liver (Böke), liver (King et al.), and liver (Rao & Gregg) compared with the calculated value of liver XCOM	126
Table 4.10	Mean attenuation values (CT number) for <i>Rhizophora</i> spp. particleboards bonded with epoxy resin (5%, 10%, and 15%), epoxy resin, distilled water, and an adult human liver	129
Table 4.11	Lesion CT number, liver CT number, lesions to liver contrast (Cn), liver noise, and contrast-to-noise ratio (CNR) measurements for the simulated liver lesions scanned with single and dual energy CT protocols	137
Table 4.12	Normality test for CT number, contrast and contrast-to-noise ratio variables	139
Table 4.13	One-way ANOVA statistical results of contrast (Cn) and contrast-to-noise ratio (CNR) measurements of four groups of original SAL images. Further details can be referred in Table J2 of Appendix J	140

Table 4.14	Lesions to liver contrast (Cn), liver noise (SD), and contrast-to-noise ratio (CNR) measurements of the liver lesions for pre-processing and post-processing SAL images using the contrast stretching technique	142
Table 4.15	Paired t-test statistical results of contrast (Cn) and contrast-to-noise ratio (CNR) measurements of eight pairs of pre-processing and post-processing SAL images before and after applying the contrast stretching technique. Further details can be referred in Table J3 of Appendix J	145
Table 4.16	Lesions to liver contrast (Cn), liver noise (SD), and contrast-to-noise ratio (CNR) measurements of the liver lesions for pre-processing and post-processing SAL images using the CLAHE technique	147
Table 4.17	Paired t-test statistical results of contrast (Cn) and contrast-to-noise ratio (CNR) measurements of eight pairs of pre-processing and post-processing SAL images before and after applying the CLAHE technique. Further details can be referred in Table J3 of Appendix J	150

LIST OF FIGURES

	Page
Figure 2.1	The liver (Chung, 2011) 12
Figure 2.2	Focal nodular hyperplasi lesion (arrow) A) lesion on the arterial-phase CT image is hyperattenuated to the liver, B) lesion on venous-phase CT image is isodense to the remainder of the liver and C) lesion on the delayed-phase image is isodense to the liver (Kamaya et al., 2009) 16
Figure 2.3	Contrast-enhanced CT images for a 64-year-old man with hepatocellular carcinoma (a small lesion): A) 140-kVp image, B) 80-kVp image, and C) averaged image generated with dual-energy CT. The 80-kVp image shows a hyperattenuated lesion (arrow), which is not identified on corresponding 140 kVp and dual-energy averaged images (Altenbernd et al., 2011) 19
Figure 2.4	Four Axial CT images of liver phantom obtained with A) (140 kVp and 225 mAs), B) (120 kVp and 275 mAs), C) (100 kVp and 420 mAs), and D) (80 kVp and 675 mAs) protocols. On A, only four lesions were detected by the three radiologists, whereas on D, all lesions can be clearly delineated (Marin. et al., 2009b) 20
Figure 2.5	Liver phantom (QRM, Mohrendorf, Germany) 15 cm in diameter contained 16 cylindric cavities (arrow). The phantom placed in a plastic container (height, 17.0 cm; semi-minor axis, 22.0 cm; semi-major axis, 25.0 cm) and filled with water 35
Figure 2.6	Liver phantom (QRM, Moehrendorf, Germany). The liver phantom (black star) with the added fat ring (white star) mimics a medium-sized patient (total diameter is 30 cm) 36
Figure 2.7	Diagram of the anthropomorphic liver phantom, which is a slab with liver insert and simulated iodinated liver lesions of two concentrations 38
Figure 2.8	Transverse CT images of A) small, B) medium, C) large, and D) extra-large phantoms containing 2 hypoattenuating lesions and one hyperattenuating lesion 39

Figure 2.9	Anthropomorphic liver phantom (ATOM Phantom, model 702CIRS). A) Photograph of small, medium, and large phantoms. B) Corresponding representative transverse 120-kVp CT image shows simulated hyperattenuating liver lesions (arrows)	41
Figure 2.10	Contrast detail phantom containing 45 cylindric lesions of five low-contrast levels and different three sizes. A) Schematic photograph and B) CT image shows overview of the phantom. The lesions arranged in groups of three with five contrast levels (1, 20 HU; 2, 15 HU; 3, 12 HU; 4, 9 HU; 5, 5 HU at 120 kVp) and three sizes (A, 6 mm; B, 4 mm; C, 2 mm)	42
Figure 2.11	Using histogram equalization with constrained variational offset method on liver CT images. Arrows point to the infected portion of liver tissue for A) Original CT image and B) enhanced CT image (Sharma & Mittal, 2015)	45
Figure 2.12	Using contrast stretching filter on liver CT images. A) Original CT image and B) enhanced CT image (Mostafa et al., 2012)	46
Figure 2.13	A, C and E images are the original liver CT images of a patient suffering from liver cancer and the cancerous part is pointed by circular marker. Images: B, D, and F are the enhanced images (post-processing images). Images: A and B contain hepatocellular carcinoma lesions and images: C, D, E, and F with metastasis lesions. The lesions are clearly visible in the enhanced images and it is easier to differentiate between normal and lesions part in the enhanced images (Thakur et al., 2016)	48
Figure 2.14	Enhancing abdomen CT images using CLAHE technique. A, B, and C images are original low-contrast abdomen CT image. D, E, and F images are corresponding enhanced images by CLAHE (Al-Ameen et al., 2015b)	50
Figure 2.15	Enhancing liver CT images using CLAHE technique. A) Original CT image and B) enhanced CT image (Krishan & Mittal, 2015)	51
Figure 3.1	<i>Rhizophora</i> spp. wood piece obtained from Kuala Sepetang, Malaysia	54
Figure 3.2	Epoxy resin product type of Resin (E-110I) and Hardener (H-9)	55

Figure 3.3	Iodine contrast medium (Omnipaque 350)	56
Figure 3.4	Calcium carbonate (CaCO ₃) in powder form	57
Figure 3.5	Instron Testing Machine (Model 5582, USA)	58
Figure 3.6	A schematic diagram (A) and Field Emission Scanning Electron Microscope (B) (model: FEI Nova SEM 450)	60
Figure 3.7	Schematic diagram of X-ray diffraction (Wakabayashi et al., 1998)	61
Figure 3.8	A schematic optical diagram (A) and fourier transform infrared spectrometer (B) (model: Thermo Scientific Nicolet iS10)	62
Figure 3.9	Structure of the NaI (Tl) detector and Photomultiplier tube	63
Figure 3.10	Schematic experimental setup for the calculation of the attenuation coefficients	63
Figure 3.11	Single Source-Dual Energy CT (SOMATOM Definition AS+, Siemens 2014)	65
Figure 3.12	Spectra of single source dual energy CT at 80 and 140 kVp energies	65
Figure 3.13	Modules and diameters of Catphan 600 phantom	66
Figure 3.14	Photo (A) and sketch drawing (B) of the QRM Liver Phantom	68
Figure 3.15	A summary of fabrication of semi-anthropomorphic liver phantom	69
Figure 3.16	A flowchart of characterization process of epoxy resin – <i>Rhizophora</i> spp. particleboards	70
Figure 3.17	<i>Rhizophora</i> spp.-epoxy resin particles preparation: A) electrical saw (Formahero FH – 600 BS), B) surface planner machine (model Holy TekHP 20), C) grinder machine (Tai-yi model, Germany), and D) grinder/mixer machine (Universal Grinding Mill DFY, 1000)	73
Figure 3.18	Digital Moisture Analyzer (model: Sartorius MA 150)	73

Figure 3.19	The <i>Rhizophora</i> spp. particleboard (30 x 20 x 0.5 cm): A) the particleboard after cold-pressing and B) the particleboard after hot-pressing	74
Figure 3.20	Dimensions and shape of the graved liver depending on adult human measurements (Riestra-Candelaria et al., 2016; Wolf, 1990)	76
Figure 3.21	Epoxy resin-iodine mixture filled in the graved liver	76
Figure 3.22	Spinal vertebra fabrication: A) 66.93% epoxy resin mixed with 33.07% CaCO ₃ and B) the epoxy resin-CaCO ₃ mixture filled in the graved vertebra	77
Figure 3.23	Photo (A) and sketch drawing (B) of the semi-anthropomorphic liver phantom (SAL) show the localizations of the simulated liver lesions	78
Figure 3.24	Mechanical testing of the particleboards: A) modulus of rupture and B) internal bond strength measurements	80
Figure 3.25	Samples immersing in distilled water for thickness swelling (TS) and water absorption (WA) measurements	81
Figure 3.26	A) Regions of interest (ROIs) of cross-sectional CT image for Catphan 600 phantom (fifth module) and B) Regions of interest (ROIs) of cross-sectional CT image for <i>Rhizophora</i> spp. particleboard bonded with epoxy resin	82
Figure 3.27	Quorum sputter coater (Q150R S)	83
Figure 3.28	The main steps of using imageJ program to image assessment and processing	93
Figure 3.29	Flowchart of the image quality analysis	94
Figure 3.30	SAL cross-sectional image showing the four regions of interest of liver lesions (ROI _{lesion} 1– 4) and three regions of interest of liver tissue (ROI _{liver} 1– 3)	96
Figure 3.31	Steps of performing contrast stretching (normalization) using ImageJ software	100
Figure 3.32	Cross-sectional SAL CT images showing the effect of contrast stretching technique on image enhancement: A) pre-processing image and B) post-processing image	100

Figure 3.33	Steps of performing Contrast Limited Adaptive Histogram Equalization (CLAHE) technique using ImageJ software	102
Figure 3.34	Cross-sectional SAL CT images showing the effect of contrast limited adaptive histogram equalization technique (CLAHE) on image enhancement: A) pre-processing image and B) post-processing image	102
Figure 4.1	Semi- anthropomorphic liver (SAL) phantom with diameters, 30 x 20 x 10 cm. A) The SAL phantom including the abdominal tissue, the liver, the spinal vertebra, and the drilled holes. B) A cross-sectional CT image of the SAL phantom including the abdominal tissue, the liver, the spinal vertebra, and the liver lesions	106
Figure 4.2	Average modulus of rupture (MOR) values of epoxy resin– <i>Rhizophora</i> spp. particleboards at different epoxy resin percentages of 0%, 5%, 10%, and 15%	109
Figure 4.3	Average internal bond (IB) strength values of epoxy resin– <i>Rhizophora</i> spp. particleboards at different epoxy resin percentages of 0%, 5%, 10%, and 15%	110
Figure 4.4	Average thickness swelling (TS) and water absorption (WA) values of epoxy resin– <i>Rhizophora</i> spp. particleboards at different epoxy resin percentages of 0%, 5%, 10%, and 15%	110
Figure 4.5	Standard deviation (SD) values of the <i>Rhizophora</i> spp. particleboards at different epoxy weight percentages (0, 5, 10, and 15%) compared with the uniform standard deviation value of Catphan 600 phantom	112
Figure 4.6	Scanning electron micrograph cross-sections of binderless <i>Rhizophora</i> spp. samples at (A) 500× and (B) 1000× magnifications and epoxy resin-bonded <i>Rhizophora</i> spp. samples at percentages of 5%: 500× (C) and 1000× (D), 10%: (E) 500× and (F) 1000×, and 15%: (G) 500× and (H) 1000×	113
Figure 4.7	XRD spectra of <i>Rhizophora</i> spp. particleboards bonded with epoxy resin at levels of 0%, 5%, 10%, and 15%	115
Figure 4.8	FTIR spectra of <i>Rhizophora</i> spp. particleboards bonded with epoxy resin at levels of 0%, 5%, 10%, and 15 %	116

Figure 4.9	Mass attenuation coefficient at a photon energy of 26.3, 59.5, and 88 keV for epoxy resin– based <i>Rhizophora</i> spp. particleboards and epoxy resin compared with the calculated XCOM of water and liver	126
Figure 4.10	Linear attenuation coefficients at photon energies of 26.3, 59.5, and 88 keV for epoxy resin sample compared with liver (Böke), liver (King et al.), liver (Rao & Gregg), and the calculated XCOM of liver	127
Figure 4.11	A, B, and C are cross-sectional CT images with two circular regions of interest (ROI-1 and ROI-2) with an area approximately 2090 mm ² for each <i>Rhizophora</i> spp. particleboards bonded with 5%,10%, and 15% epoxy resin, respectively. The D cross-section CT image shows one circular region of interest (2006.2 mm ²) of each distilled water and epoxy resin	130
Figure 4.12	Average CT number values of epoxy resin mixed with iodine concentrations of 0.0, 0.5, 0.7, 0.9, 1.1, 1.3, and 1.5 mg Iodine/g epoxy resin	132
Figure 4.13	Average CT number values of the diluted iodine solutions with concentrations of 4.2, 4.4, 4.6, and 4.8 mg Iodine/ml	133
Figure 4.14	A cross-sectional CT image of the SAL phantom showing the average CT number values of the simulated lesions. The CT number values with varying concentrations of the iodinated solutions: 4.2, 4.4, 4.6, and 4.8 mg Iodine/ml were: 102.5±10.2, 106.6±9.3, 110.3±8.7, and 113.4±8.8 HU, respectively	133
Figure 4.15	Four transverse CT images of SAL phantom obtained with: A) protocol A (80 kVp and 541 mAs), B) protocol B (100 kVp and 255 mAs), C) protocol C (120 kVp and 149 mAs), and D) protocol D (mixed energies: 80 kVp with 233 mAs, and 140 kVp with 55 mAs)	137
Figure 4.16	Transverse CT images of SAL phantom enhanced by the contrast stretching technique	143
Figure 4.17	Transverse CT images of SAL phantom enhanced using CLAHE technique.	148

- Figure 4.18 Contrast values (Cn) before and after modifying contrast stretching and CLAHE methods (pre-processing and post-processing) of the scanned liver lesions with protocol A (80 kVp and 541 mAs) 153
- Figure 4.19 Contrast noise ratio values (CNR) before and after modifying contrast stretching and CLAHE methods (pre-processing and post-processing) of the scanned liver lesions with protocol A (80 kVp and 541 mAs) 154

LIST OF ABBREVIATIONS

AAPM	American Association of Physicists in Medicine
ANOVA	One-Way Analysis of Variance
ASIR	Adaptive Statistical Iterative Reconstruction
ASIR-V	Adaptive Statistical Iterative Reconstruction Technique
CaCO ₃	Calcium Carbonate
CAD	Computer Aided Diagnostic
CHNSO	Carbon Hydrogen Nitrogen Sulfur Oxygen
CIRS	Computerized Imaging Reference Systems
CLAHE	Contrast Limited Adaptive Histogram Equalization
Cn	Contrast
CNR	Contrast-to-Noise Ratio
CT	Computed Tomography
CTDI _{vol}	Computed Tomography Dose Volume Index
CTP 600	Catphan 600 Phantom
DE	Dual Energy
DICOM	Digital Imaging and Communications in Medicine
FBP	Filtered Back Projection
FESEM	Field Emission Scanning Electron Microscope
FTIR	Fourier-Transform Infrared Spectrometer
FWHM	Full Width at Half Maximum
HE	Histogram Equalization
HU	Hounsfield Unit
IB	Internal Bond
ICRU	International Commission on Radiation Units and Measurements

IPPT	Hospital Perubatan dan Pergigian Termaju
IR	Iterative Reconstruction
JIS	Japanese Industrial Standard
KBr	Potassium Bromide
keV	Kiloelectron Volt
kVp	Peak Kilovoltage
mAs	Tube Current Time
MBIR	Model-Based Iterative Reconstruction
mg	Milligrams
MRI	Magnetic Resonance Imaging
N	Newton
°C	Degree Celsius
P	Probability
QRM	Quality Assurance in Radiology and Medicine
ROI	Region of Interest
SAL	Semi-Anthropomorphic Liver
SD	Standard Deviation
SE	Single Energy
TS	Thickness Swelling
WA	Water Absorption
XCOM	Photon Cross Sections Database
XRD	X-Ray Diffraction
Z_{eff}	Effective Atomic Number
μ	Linear Attenuation Coefficient
μ/ρ	Mass Attenuation Coefficient
^{109}Cd	Cadmium-109
^{241}Am	Americium-241

**FANTOM HATI SEMI-ANTROPOMORFIK *RHIZOPHORA* SPP. DAN
RESIN EPOKSI UNTUK PENAMBAHBAIKAN LESI HATI DI DALAM
TOMOGRAFI BERKOMPUTER**

ABSTRAK

Penyelidikan ini bertujuan membangunkan satu fantom hati separa-antropomorfik untuk tujuan mengkaji teknik pasca pemrosesan imej bagi meningkatkan kebolehlihatan lesi hati ke atas imej yang diimbas secara pelbagai protokol tomografi berkomputer. Papan partikel *Rhizophora* spp. dan resin epoksi dinilai untuk digunakan sebagai bahan-bahan asas, untuk membangunkan satu fantom hati dengan 16 lesi hati berbentuk silinder. Pelbagai peratusan resin epoksi (0%, 5%, 10%, dan 15%) ditambah kepada papan partikel untuk meningkatkan kekuatan, ciri-ciri fizikalnya dan radiologikalnya. Kepadatan jisim dan nombor atom efektif (Z_{eff}) papan partikel dan bahan resin epoksi ditentukan. Ciri-ciri radiologikal papan partikel dan bahan resin epoksi dijalankan melalui pengukuran pekali pengecilan linear dan jisim pada tenaga photon 26.3, 59.5, dan 88 keV, diikuti dengan pengukuran nombor CT pada voltan tiub 120 kVp. Fantom diimbas menggunakan empat protokol imbasan CT (80 kVp, 100 kVp, 120 kVp, dan dwi-tenaga CT) pada aras dos radiasi yang malar. Nilai kontras dan nisbah kontras kepada hingar kemudian ditentukan. 'contrast stretching' dan teknik-teknik 'CLAHE' digunapakai ke atas imej-imej CT yang diperolehi dengan tujuan meningkatkan kebolehlihatan lesi hati. Dapatan menunjukkan bahawa penambahan resin epoksi 15% telah meningkatkan lagi kekuatan, keseragaman, morfologi, kehabluran, indeks dan fizikal, serta ciri-ciri radiologi papan partikel dalam

menyamai tisu badan di bahagian abdomen. Melalui teknik ini, papan partikel mencapai kepadatan jisim 1.03 g/cm^3 dan Z_{eff} of 7.16. Keputusan pekali pengecilan menunjukkan bahawa papan partikel yang ditambah dengan resin epoksi sebanyak 15% sesuai untuk menyamai tisu lembut. Nombor CT pada papan partikel berjulat di antara 20.5 kepada -25.2 HU, yang berada dalam julat nombor CT tisu lembut. Pengukuran ciri-ciri fizikal dan radiologikal menunjukkan bahawa resin epoksi adalah sesuai untuk menyamai tisu hati dengan kepadatan jisim 1.11 g/cm^3 dan Z_{eff} 7.11. Apabila dibandingkan dengan nilai rujukan bagi tisu hati, perbezaan relatif pengukuran μ dan μ/ρ untuk resin epoksi berada dalam julat 2.2% sehingga 10.97%. Nombor CT resin epoksi berada pada 69.2 HU, iaitu hampir dengan nombor CT rujukan pada tisu hati (57 - 66 HU). Keputusan imbasan menunjukkan bahawa kontras (Cn) dan nisbah kontras kepada hingar (CNR) lesi hati adalah lebih tinggi pada voltan tiub yang rendah, terutama pada protokol 80 kVp. Secara statistik, kajian ANOVA sehala menunjukkan bahawa lesi hati pada imej CT yang diperolehi pada 80 kVp, adalah lebih baik dari nilai-nilai Cn dan CNR berbanding dengan tiga protokol lain (nilai $P < 0.05$). Pengukuran Cn dan CNR menunjukkan bahawa 'contrast stretching' dan teknik-teknik CLAHE yang diaplikasi kepada imej-imej CT diperolehi pada 80 kVp menunjukkan peningkatan kebolehlihatan lesi yang paling ketara dengan nilai-nilai P ujian-t < 0.05 . Keputusan-keputusan kualitatif dan kuantitatif menunjukkan bahawa peregangan kontras adalah teknik yang terbaik untuk meningkatkan lesi hati Cn dan CNR. Sebagai kesimpulan, kebolehlihatan lesi hati yang hyper dan dengan kontras yang rendah didapati paling bermutu tinggi apabila ia diperolehi pada 80 kVp dengan dipasca-proses lebih lanjut menggunakan teknik peregangan kontras.

***RHIZOPHORA* SPP. AND EPOXY RESIN BASED SEMI-
ANTHROPOMORPHIC LIVER PHANTOM FOR LESIONS
ENHANCEMENT IN COMPUTED TOMOGRAPHY**

ABSTRACT

This study aims to construct a semi-anthropomorphic liver phantom for the purpose of investigating image post-processing techniques to improve the visibility of liver lesions on images scanned at various computed tomography (CT) protocols. *Rhizophora* spp. particleboards and epoxy resin were evaluated to be used as basic materials, which construct a liver phantom with 16 cylindrical liver lesions. Various percentages of epoxy resin (0%, 5%, 10%, and 15%) were added to the particleboards to improve their strength, physical and radiological properties. Mass density and effective atomic number (Z_{eff}) of the particleboards and epoxy resin materials were determined. Radiological properties measurement of the particleboards and epoxy resin were carried out via measurement of linear (μ) and mass attenuation (μ/ρ) coefficients at photon energies 26.3, 59.5, and 88 keV, followed by CT number measurements at tube voltage 120 kVp. The phantom was scanned by using four CT scanning protocols (80 kVp, 100 kVp, 120 kVp, and dual energy CT) at a constant radiation dose level. The contrast (Cn) and contrast-to-noise ratio (CNR) of the acquired images were then determined. Then, contrast stretching and contrast limited adaptive histogram equalization (CLAHE) techniques were applied with an aim to further improved the visibility of the lesions. The results showed that the addition of 15% epoxy resin has enhanced strength, uniformity, morphology, crystallinity index, physical, as well as the radiological properties of the particleboard to mimic

abdominal body tissues. The mass density of the particleboard is 1.03 g cm^{-3} , with Z_{eff} equivalent to 7.16. The attenuation results showed that the particleboard, which was bonded with 15% epoxy resin, is suitable for mimicking physical and radiological properties of soft tissue. The CT number of the particleboard was found to be ranging from -20.5 to -25.2 HU, which is within the range of CT number of soft tissues. The physical and radiological properties measurements showed that the epoxy resin is suitable to mimic the liver tissue with mass density of 1.11 g cm^{-3} and Z_{eff} of 7.11. When compared to the reference values of liver tissue, the relative differences of μ and μ/ρ measurements of the epoxy resin were found to be ranging from 2.2% to 10.97%. The CT number of the epoxy resin was found to be 69.2 HU, which is close to the reference CT number of liver tissue (57 to 66 HU). The scanning results showed that Cn and CNR of liver lesions were higher at low tube voltages, particularly at 80 kVp protocol. Statistically, a one-way analysis of variance (ANOVA) study showed that liver lesions on CT images that were acquired at 80 kVp, were significantly superior in their Cn and CNR values compared to the three other protocols (P values < 0.05). The Cn and CNR measurements showed that the contrast stretching and CLAHE techniques that were applied on the CT images acquired at 80 kVp had the utmost lesions visibility improvement with t-test P values < 0.05. The qualitative and quantitative results showed that the contrast stretching is the best technique to enhance the Cn and CNR of liver lesions. In conclusion, the visibility of low contrast small hyperattenuating liver lesions was found to be at its uppermost quality when it is acquired at 80 kVp and post-processed further by using the contrast stretching technique.

CHAPTER 1

INTRODUCTION

1.1 Introduction

Phantom is a designed object that mimics the human body in medical imaging examinations to evaluate, analyze, and tune the performance of various imaging devices. Phantom materials can range from water to complex mixtures, used to mimic physical properties of ionizing radiation as it interacts with human tissues. It is conveniently used in radiological studies such as dosimetry measurements, radiotherapy studies, quality assurance, and quality control procedures. Water is a standard phantom material as it has perfect physical properties that match the human's soft tissue in low and high energy ranges. Water has a liquid state and, therefore, it cannot always be performed as a phantom material in medical imaging studies. As a result, several solid materials such as polystyrene, Perspex, as well as different types of polymers were developed as a phantom material to be used in medical imaging studies. The use of these phantom materials, however, does not yield precise results compared with water because they fail to simulate true value of physical and radiological properties of tissues. Therefore, further studies were carried out by the medical physics community to develop more precise and accurate phantom materials to be used in medical imaging fields or related studies (DeWerd & Kissick, 2014).

A Rhizophora is a type of mangrove hardwood that can be found growing in tropical and subtropical countries. Previous studies confirmed the suitability of

Rhizophora species (*Rhizophora* spp.) as phantom materials (Bradley et al., 1991; Sudin et al., 1988; Tajuddin et al., 1996). The use of *Rhizophora* spp. in a particleboard form has better properties compared with untreated raw wood in the purpose of phantom fabrication (Marashdeh et al., 2012). However, particleboards suffer a reduction in physical and mechanical properties against solid raw wood. Therefore, a new method of fabrication is implemented in studies by adding adhesives into the *Rhizophora* spp. particleboard to improve their strength and at the same time maintain their attenuation characteristics (Ababneh et al., 2016; Abuarra et al., 2014; E. T. Tousi et al., 2014; Yusof et al., 2017). Nevertheless, using some adhesives in particleboard phantom materials fabrication was found to be unsuccessful to produce a good simulation compared with water at different energy levels (Ngu et al., 2015; Surani, 2008). Therefore, to fabricate a *Rhizophora* spp. particleboard, it is necessary to select an appropriate wood adhesive with specific characteristics to enhance the mechanical, physical and radiological properties of the particleboards so that a new suitable phantom material is provided and can be used in CT studies.

Epoxy resin, also called polyepoxide, is a type of reactive polymer and prepolymer that contains epoxide groups. It reacts with too many co-reactants such as phenols, amines, and thiols or to themselves in the presence of catalysts (Pascault et al., 2002). Epoxy resins have excellent physical, chemical and mechanical properties, not toxic, and can bond in high strength with other materials (DeWerd & Kissick, 2014; Strzelec, 2007). They are used in medical imaging studies because of their high quality and great reproducibility (Singh, 2014; White et al., 1977). Such characteristics of the epoxy resin make it seem like an appropriate binder material

enhancing the mechanical, physical and radiological properties of the *Rhizophora* spp. particleboard, and as a main phantom material to mimic the physical and radiological properties of the human's liver tissue in CT studies.

Medical imaging refers to various types of imaging techniques that are utilized to analyze and observe the human body to diagnose, treat or monitor medical conditions. CT scan is the first medical imaging modality, which used an X-ray with a computer to produce detailed images about the scanned area (Farncombe & Iniewski, 2013). CT number reflects the average linear attenuation coefficients of the cross-section CT images depending on the scanned region properties including chemical composition, density, atomic number, and beam filtration (Bryant et al., 2012). Therefore, CT phantom materials should have close X-ray attenuation coefficients and CT number values as in the human tissues. As a result, characterizing a tissue equivalent material in CT depends highly on its attenuation properties that are related to the clinical CT tube energy ranging between 80 – 140 kVp (40 – 65 keV) (Huda et al., 2000; Yohannes et al., 2012).

The liver has specific physical and attenuation characteristics that help provide more diagnostic details in CT examinations such as injuries, infections, lesions diagnosis, and other diseases (Venkatesh et al., 2014). Therefore, many researchers used liver phantoms to improve image quality, reduce radiation dose level, and diagnose different pathological types in CT liver examinations (Euler et al., 2017; Grant et al., 2014; Husarik et al., 2014; Marin et al., 2016; Martinsen et al., 2008).

The detection of liver lesions in a CT examination is directly related to the lesion to liver contrast. Therefore, quantitative measurements as contrast and contrast to noise ratio are often utilized to evaluate the image quality and liver lesions visibility in CT liver examinations. Hyperattenuating liver lesions are usually seen during the so-called late arterial phase when lesions are maximally enhanced by the injected iodine contrast agent, whereas there is a minimal enhancement of the surrounding liver tissue (Kamaya et al., 2009). As verified by the results of several studies, the administration of iodine contrast material has enhanced lesion to liver contrast effectively during the late arterial phase protocol (Johnson et al., 2015; Schindera et al., 2008; Takahashi et al., 2002).

Distinguishing between low contrast liver lesions and liver tissue is extremely important because the lesions as well as the normal area of the liver are presented with overlapping intensity distributions due to their close attenuation values. This means that similar CT number values can be provided for two different materials at a given energy (e.g., liver lesions and liver tissue). Lesions and the surrounding liver tissue contain different iodine concentrations in late arterial phase protocol. Therefore, changing the tube energy settings may provide new different linear attenuation coefficient values that help increase the contrast ratio between the lesions and the liver tissue. To take advantage of the inherent attenuation property of iodinated contrast material, the increased iodine attenuation (lesions contrast) can be introduced by decreasing tube voltage values to be closer to the k-edge of iodine (33.2 keV) (Marin. et al., 2009b; Marin. et al., 2009a). However, different studies showed that the low contrast small liver lesions (less than 2 cm) are not often detectable as the large lesions on CT liver examinations. These studies showed the

poor quality of the CT image to attain an early diagnosis of small size liver lesions (Abraham-Nordling et al., 2017; Brancatelli et al., 2001; Monzawa et al., 2007; Pazgan-Simon et al., 2015). Further studies are, therefore, required to enhance the diagnosis of low contrast small liver lesions in CT examinations.

In the field of medical image processing, contrast enhancement methods play a vital role in producing an image that is clearly recognizable for different medical imaging applications. Enhancing small liver lesions contrast in CT examinations is important to increase the diagnostic performance of these lesions and provide the best treatment. Contrast enhancement techniques function to change pixel intensity values for enhanced images to help medical practitioners in making more informed diagnoses. The contrast enhancement methods are often modified to change the dynamic range of pixel intensity values to enhance the image quality. These methods function to remap the grayscales of the input image (the pre-processing image) so that the grayscales of the output image (the post-processing image) results in the enhancement of the subjective image quality for the output image. The new peaks in image histogram may increase the contrast of region of interest for the post-processing image compared with the pre-processing image (Lo & Puchalski, 2008; Min et al., 2013). This means that contrast enhancement techniques can be performed on the grayscale CT image to improve the image quality and increase the diagnostic possibility of small liver lesions. This study aims to construct a specific semi-anthropomorphic liver phantom to investigate image enhancement techniques so that the visibility of low contrast small hyperattenuating liver lesions that are scanned at various CT protocols is enhanced.

1.2 Problem Statement

Although water is the primary phantom material as it has perfect physical and attenuation properties that are matching the human's soft tissue, the state of existence of water does not always make it practical to be used as a tissue equivalent material. For this reason, many solid phantom materials such as wood, polystyrene, and Perspex were developed. However, such materials have several limitations to be used as tissue equivalent materials in CT applications due to variations in their chemical composition, attenuation properties, effective atomic number, and CT number values (Yohannes et al., 2012). In addition, some of these materials like wood have a few limitations due to changes in attenuation properties, moisture content, water absorption and the ability to crack. For example, the attenuation coefficient measurements of the *Rhizophora* spp. particleboards bonded with formaldehyde adhesives were not in agreement with water values. The attenuation properties of these particleboards at 59.5 keV photon energy were significantly far from that of the breast tissue (Ngu et al., 2015; Surani, 2008).

In clinical CT liver examinations, iodine contrast agent is injected into patients to enhance the CT image quality. The injected iodine increases the CT number value and changes the chemical composition of the liver tissue. The composition of commonly used liver tissue equivalent materials does not contain iodine, which makes these materials unsuitable to mimic the actual CT number and chemical composition of the human's liver tissue during CT iodinated protocols. Moreover, the available CT liver phantoms are considered laborious, which require special software, specific sizes and shapes according to the experiment required.

Therefore, it is necessary to construct a liver phantom with appropriate tissue equivalent properties to be used in CT liver examinations (Grant et al., 2014; Husarik et al., 2015).

Hyperattenuating liver lesions are usually seen during late arterial phase protocol when lesions are maximally enhanced by the injected iodine contrast agent. However, the CT image contrast is still considered to be relatively insensitive in the depiction of small liver lesions (less than 2 cm), particularly when the lesions have a CT number that is close to the liver tissue (low contrast lesions). The identification of low contrast liver lesions from CT images is challenging due to the low contrast between the lesions and the liver tissue. These lesions are frequently mistaken as they typically show rapid homogeneous uptake of iodine contrast with a rapid return to near-normal enhancement (Abraham-Nordling et al., 2017; Brancatelli et al., 2001; Monzawa et al., 2007; Pazgan-Simon et al., 2015). Therefore, enhancing the lesions' contrast and visibility is important to increase the possibility of early diagnosis and provide the best treatment. Because the lesions and the liver tissue contain different iodine concentrations in late arterial phase protocol, changing the tube energy settings will provide new attenuation measurements (CT number values), which may help increase the visibility of these lesions (Lusic & Grinstaff, 2012).

The low contrast in CT image has an impact on the process of pathologic diagnosing. There is, however, a limitation in the CT images in the visualization of their textural details. The low contrast liver lesions have grayscale values that are close to the grayscale values of the liver tissue and, thus, they occupy only a relatively narrow range of the grayscale of pixels. The low differences between the

grayscale values make lesions' detection more difficult to be delineated by the human eye. This means that the lesions and the liver tissue have similar pixel intensity values, which have an impact on the diagnostic possibility of these lesions (Lamba et al., 2014). Therefore, the enhancement methods to expand the contrast of the scanned area's pixels may help improve the discrimination between liver lesions and the liver tissue to make the low contrast lesions more detectable.

1.3 Research Objectives

This study primarily aims to construct a semi-anthropomorphic liver phantom to investigate image contrast enhancement techniques to improve the visibility of liver lesions on images that are acquired by using CT scanners. To achieve the main goal of the study, it is important to formulate a specific phantom that simulates the attenuation properties of liver lesions, liver tissue, and its surrounding tissues. The specific objectives of the study are as follows:

1. To study the stability, strength, internal structure of tissue equivalent material that mimics liver's surrounding tissues.
2. To determine the physical and radiological properties of tissue equivalent materials to simulate liver tissue and its surrounding tissues.
3. To develop a semi-anthropomorphic CT liver phantom to mimic attenuation properties of liver lesions, liver tissue and its surrounding tissues for intermediate weight patient during late arterial phase protocol.
4. To investigate the effect of CT tube voltages on contrast and contrast-to-noise ratio of the lesions embedded in the phantom.
5. To investigate the usage of contrast stretching and contrast limited adaptive histogram equalization (CLAHE) contrast enhancement techniques to improve the contrast and contrast-to-noise ratio of the lesions embedded in the phantom.

1.4 Scope of the Study

In this study, the selected phantom materials, which are equivalent to the human liver and abdominal body tissues are used to formulate a semi-anthropomorphic CT liver phantom. Iodine solutions are inserted in the liver to simulate low contrast small hyperattenuating liver lesions. Epoxy resin is added to *Rhizophora* spp. particleboards to improve the stability, strength, internal structure of the tissue equivalent material that mimics the liver's surrounding tissues. The formulated phantom is scanned at various CT protocols to conclude the tube energy that best shows liver lesions' visibility. By using the ImageJ software, contrast stretching and CLAHE post-processing techniques were applied to enhance contrast and contrast-to-noise ratio of the acquired CT images. The optimum tube setting and post-processing technique to improve the visibility of liver lesions' diagnosis in CT liver examinations are recommended at the end of this study. This study was carried out with an aim to improve the visibility of liver lesions in arterial phase protocol by changing tube setting values. The other protocols parameters such as, slice thickness, algorithm filters, and tube rotation time were not studied. Moreover, the contrast and contrast-to-noise ratio indexes were determined in this study to evaluate the image lesion visibility. Other indexes of CT image quality such as spatial resolution and beam hardening artifact were not evaluated in this study.

The important limitations of this study are outlined as the following:

1. The attenuation of the phantom represents a homogeneous late arterial phase CT liver protocol. It does not include heterogeneous areas, which might be present in patients with other liver diseases.

2. The study simulated only one type of liver lesions, i.e., hyperattenuating cylindrical lesions.
3. The phantom simulated an adult patient with an abdominal cross-section mimicking a medium body size. The study did not consider the differences in body sizes.
4. The dual energy CT, which is used in this study, is limited to a fixed energy combination 80 and 140 kVp.

1.5 Structure of the Thesis

The overall structure of this thesis takes the form of five chapters. The first section of chapter 1 describes the using of phantom materials in medical physics studies and discusses the role of CT imaging and image enhancement techniques in the detection of liver lesions. The problem statement, objectives, and scope of this research are mentioned briefly in the sections: 1.2, 1.3 and 1.4, respectively. Chapter 2 presents an overview of previous researchers that are associated with the goals of current study. Chapter 3 focuses on the materials and methodology used in this study, includes how the phantom was fabricated and how scanning procedures were performed on the phantom. Chapter 3 also explains the process of modifying contrast stretching and CLAHE contrast enhancement techniques by using imageJ software. Chapter 4 presents the findings of the research, focusing on the mechanical, physical, and radiological properties of the fabricated phantom. Qualitative and quantitative assessments of the scanned liver lesions before and after post-processing techniques were also discussed in this chapter. Finally, chapter 5 summarizes the conclusions and main areas covered in this research. Limitations of the study and suggestions for future improvements and directions for next researchers are also discussed.

CHAPTER 2

THEORY AND LITERATURE REVIEW

This chapter provides a critical overview about published works that are associated with the objectives and research problems of this research study. This chapter also explains the role of liver phantoms in liver lesions studies. The currently available CT phantoms that are used in CT liver examinations are highlighted in this chapter. The role of CT image enhancement techniques in CT imaging is also discussed at the end of this chapter.

2.1 The Liver

The liver is the biggest organ inside the human body (Figure 2.1). It is irregularly shaped and extends from the upper right of the abdomen and part way into the left upper side. It is located below the heart and the lungs, and to the right of the spleen, there are the stomach and intestine. The liver consists of four lobes. They are right, left, caudate, and quadrate lobes. The right and left lobes are separated by the falciform ligament. The small caudate lobe extends posteriorly from the right lobe. The small quadrate lobe is located below the caudate lobe and extends posteriorly from the right lobe. The liver performs many essential functions that are related to digestion, metabolism, immunity and the storage of nutrients within the body. These functions make the liver an important human organ (Derrickson & Tortora, 2007; Marieb & Hoehn, 2007). The liver occupies 2.5% of the adult body weight (approximately 1.4 to 1.5 kg) (Riestra-Candelaria et al., 2016). Table 2.1 shows the size and dimensions of adult human liver.

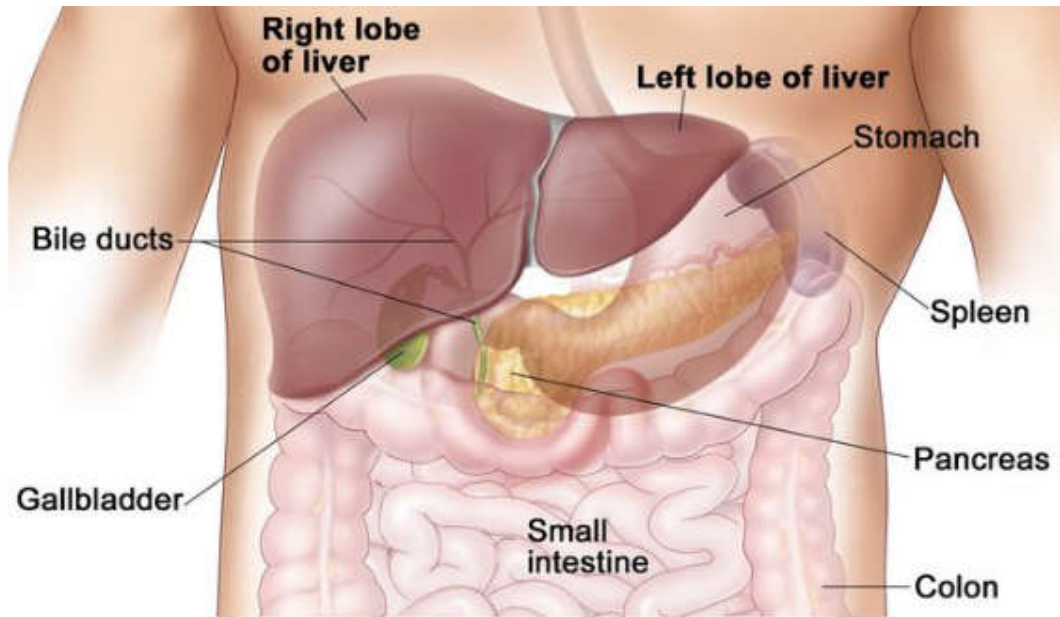


Figure 2.1 The liver (Chung, 2011)

Table 2.1 Dimensions of adult human liver

Liver Length (cm)	Location of liver Measurements	Reference
13.3 to 15.5	Midhepatic Line	(Gosink & Leymaster, 1981)
15.5	Medhepatic Line	(Riestra-Candelaria et al., 2016)
13-17	Longitudinal scan at midclavicular line	(Curry & Tempkin, 2015)
15-20 cm	Longitudinal scan under the costal margin from the inferior tip of the liver to the dome of the diaphragm in an oblique line	(Stephenson, 2012)
12.5	Craniocaudal Plane	(Riestra-Candelaria et al., 2016)
10.5-13.5	Midclavicular Line:	(Riestra-Candelaria et al., 2016)
12.5-14.9	Vertical line (Midaxillary Line)	(Riestra-Candelaria et al., 2016)

2.1.1 Liver Lesions

Liver lesions can either be benign or malignant. These lesions are divided into four categories: hypovascular lesions, hypervascular lesions, cystic lesions, and fat-containing lesions. The incidence of liver lesions has increased over the last few decades. This is mainly because of the improved cross-sectional medical imaging techniques, which have enhanced the detection rate of the lesions. The widespread of cross-sectional medical imaging techniques (CT and MRI) have contributed in increasing the diagnostic possibility of liver lesions. The diagnosis of liver lesions, especially in early stages, is important for optimal patient management and treatment (Jemal et al., 2010; Manfredi et al., 2006; Torre et al., 2015).

The most frequent benign liver lesions of the epithelium origin are a hepatocellular adenoma, and focal nodular hyperplasia in addition to those of the mesenchymal origin, which are angiomyolipoma and haemangioma. Benign lesions such as haemangioma and focal nodular hyperplasia rarely increase in volume and often do not require any treatment (Choi et al., 2005; Nault et al., 2013). Although angiomyolipoma and hepatocellular adenoma lesions are true neoplastic lesions, better knowledge of their natural history and understanding of their pathological and radiological properties has resulted in a decrease in the use of resection for diagnosis (Dokmak et al., 2009).

The malignant liver lesions can either consist of metastases from other malignancies like breast cancer metastases and colorectal liver metastases, or primary hepatic malignancies like intrahepatic cholangiocellular carcinoma and hepatocellular carcinoma (most frequent primary malignancy of the liver). Treatment of malignant liver lesions differs widely and ranges from no treatment, resection,

follow up, chemotherapy, radiofrequency ablation or a combination thereof. To apply the best treatment strategy, an adequate characterization and detection of these lesions with non-invasive medical imaging techniques are important (Befeler & Di Bisceglie, 2002; Liang et al., 2009; Loudin et al., 2017). In treating patients with malignant liver lesions, it is critical and important to detect the lesions at an early stage to avoid unnecessary surgery, and select patients, who will benefit from curative liver resection (Albiin, 2012; Algarni et al., 2016).

2.1.1.1 Liver Lesions Diagnosis in CT Examinations

CT scan has become an important radiologic modality in diagnostic radiology departments since the 1970s when it was first introduced. CT is a medical imaging technique that uses the computer to process multiple X-ray projections that are taken from different angles. The computer converts signals that are acquired by detectors to produce a series of detailed cross-sectional images of areas inside the body. These images precisely provide 3-D views of certain parts of the scanned area such as blood vessels, soft tissues, the brain, the lungs, the liver, and the bones. Therefore, CT is often the most preferred modality of diagnosing different pathological types like many cancers, bone and traumatic injuries, infections, and cardiovascular diseases (Hsieh, 2009; Seeram, 2015).

Over the last few decades, major enhancements have occurred in the liver imaging. Magnetic Resonance Imaging (MRI) and CT are currently the primary medical imaging modalities that are performed to diagnose liver lesions. These modalities have a good potential to improve the detection and characterization of the liver lesions (Inan et al., 2010). However, CT remains the best modality for the liver lesions' imaging due to its high detection sensitivity in the evaluation of suspected

liver lesions. It also offers good accuracy and exceptional resolution of the lesions' diagnosis. Intravenous iodinated contrast media technique is improved the contrast of liver lesions and thus aid in the detection of these lesions. This preference is largely attributable to the effects of the iodine contrast on the enhancement characteristics of lesions, as compared with normal liver tissue. Thus, CT is the imaging modality of choice for evaluating different types of liver lesions (Algarni et al., 2016; Choi, 2006; Murakami et al., 2011).

The conspicuity of the liver lesions on diagnostic imaging examinations mainly depends on an adequate contrast with the normal liver tissue. CT liver scanning is usually performed after injection of iodine contrast agent to attain adequate lesion to the liver contrast. Intravenous contrast is injected into a vein in CT examinations to enhance the visibility of blood vessels and tissue structure of various organs. CT scanning pre and post-intravenous administration of iodine is an excellent way of evaluating different types of liver lesions. The post-contrast evaluation can be performed in three stages of enhancement. These stages include the arterial phase, the portal venous phase, and the delayed phase (Begum et al., 2016; El-Serag, 2001; Kamaya et al., 2009).

The highest lesion to liver contrast is often seen during the late arterial phase protocol when lesion neovascularity maximally enhances, while there is a minimal enhancement of the surrounding liver tissues. Kamaya et al. (2009) demonstrated that the late arterial-phase protocol improved the liver lesions' visibility by increasing the contrast enhancement of the liver lesions in comparison with the liver tissue (hyperattenuating lesions). The study evaluated the liver lesions' visibility using liver CT images, which are obtained in the late arterial-phase, the portal-venous phase,

and the delayed-phase protocols. The late arterial-phase CT image of the liver provided the best lesion visibility as shown in Figure 2.2. The images showed that there is a significant difference in the mean attenuation of the enhanced liver lesion (hyperattenuating lesion) compared with the liver tissue.

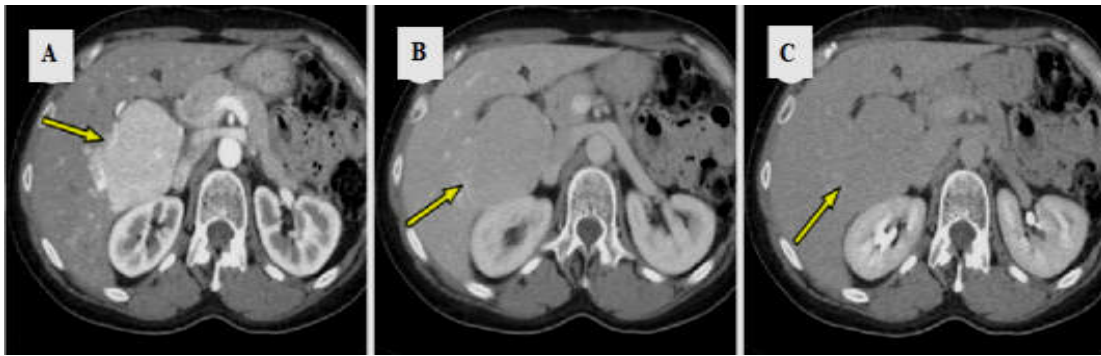


Figure 2.2 Focal nodular hyperplasi lesion (arrow) A) lesion on the arterial-phase CT image is hyperattenuated to the liver, B) lesion on venous-phase CT image is isodense to the remainder of the liver and C) lesion on the delayed-phase image is isodense to the liver (Kamaya et al., 2009)

Based on previous studies in the literature, using the late arterial phase for the evaluation of the hypervascular liver lesions has increased the possibility of an earlier detection and improved the lesions' treatment potentiality (Johnson et al., 2015; Schindera et al., 2008; Shuman et al., 2014; Takahashi et al., 2002). These studies clarified that the optimization of the late arterial phase imaging is important to improve the conspicuity of the liver lesions' diagnosis.

2.1.1.2 The Effect of CT Tube Voltage Setting on Liver Lesions' Diagnosis

Tube voltage describes the energy of the photon (beam quality) in kilo voltages unit (kVp). The changing in the tube energy must be low and reasonably achievable with the image quality and the radiation dose level. To produce CT images with the highest contrast to the surrounding tissue, the tube energy can be adjusted to closely

match the absorption edge (k-edge value) of the relevant imaging agent atoms (i.e., iodine) (Lusic & Grinstaff, 2012). Nevertheless, decreases in kVp can be partially offset by the higher image noise level and CT image artifacts that occur at low kVp settings due to a combination of reduced photon energy and flux. This problem can be solved by adjusting the scanning protocol parameters such as increasing the tube current time (mAs) (Primak et al., 2006; Sigal-Cinqualbre et al., 2004).

The reduction in the tube voltage setting has increased the contrast enhancement of CT image in iodinated CT examinations because of approaching the k-edge of iodine. Therefore, many studies, which evaluated the use of low kVp in different CT protocols, have shown that such a reduction can obviously improve the CT image quality and reduce the radiation dose level in different CT examinations (Clark & Gunn, 2017; Dong et al., 2012; Feuchtner et al., 2010; Gnannt et al., 2012; Taguchi et al., 2017). It is now widely accepted that low-kVp CT protocols are the most helpful in improving the attenuation of iodine to be useful in terms of image contrast (McCollough et al., 2012). A review of the previous related studies is outlined in Table 2.2. These studies concluded that single energy (SE) and dual-energy (DE) CT protocols have successfully confirmed that changing the tube energy can improve the delineation of various types of liver lesions.

Table 2.2 Summary of the literature about tube voltage (kVp) settings capability in assessing the conspicuity of different types of liver lesions

Liver Lesions' Diagnosis	Findings	Reference
Hepatocellular carcinoma and metastasis	80 kVp enhanced conspicuity of malignant hypervascular liver lesions in comparison with 140 kVp.	(Marin. et al., 2009b)
Metastasis	Enhanced attenuation differences between liver lesions and liver tissue at 80 kVp compared with 120 kVp.	(Robinson et al., 2010)
Hepatocellular carcinoma	50-keV images improved liver lesion conspicuity compared with 77 keV images.	(Shuman et al., 2014)
Uveal melanoma	80-kVp images more sensitive in liver lesion detection than 120 kVp image. Low-kVp images of dual-energyCT are more sensitive in detecting liver lesions than virtual 120 kVp images.	(Altenbernd et al., 2016)
Hepatocellular carcinoma, metastasis, and cysts	50-keV images show higher diagnostic performance over 120 kVp-equivalent images.	(Caruso et al., 2017)

To study the effect of low energy in the hepatic arterial phase images, Altenbernd et al. (2011) evaluated the contrast-enhanced in liver CT images, which are obtained at 140-kVp, 80-kVp and an averaged image that is generated with DECT. The results confirmed that the low energy arterial phase images have higher attenuation within the hyperattenuating liver lesions in comparison with the liver tissue and, therefore, the conspicuity of these lesions has increased. As shown in Figure 2.3, the contrast-enhanced CT images that are obtained with 80 kVp have higher improvements in the attenuation of liver lesions compared with the 140 kVp and the averaged DECT images.

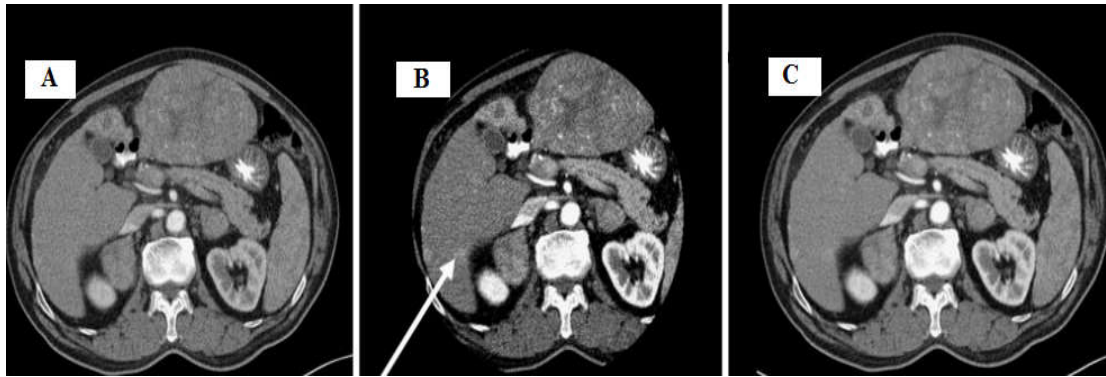


Figure 2.3 Contrast-enhanced CT images for a 64-year-old man with hepatocellular carcinoma (a small lesion): A) 140-kVp image, B) 80-kVp image, and C) averaged image generated with dual-energy CT. The 80-kVp image shows a hyperattenuated lesion (arrow), which is not identified on corresponding 140 kVp and dual-energy averaged images (Altenbernd et al., 2011)

In a phantom study, Marin-Daniele et al. (2009) investigated the effect of a low tube voltage combined with high tube current on image noise, CNR, lesion visibility, and radiation dose level. The phantom, which contains 16 cylindrical cavities to simulate hyperattenuating liver lesions, is scanned at 140, 120, 100, and 80 kVp, with corresponding mAs settings at 225, 275, 420, and 675 mAs, respectively. The statistical analysis included a one-way analysis of variance (ANOVA) test. The results indicated that a reduction of tube voltage from 140 to 120, 100, and 80 kVp increased the CNR by factors of 1.6, 2.4, and 3.6, respectively ($P < .001$). The results also concluded that the highest lesion conspicuity is achieved with the 80-kVp protocol (Figure 2.4). Accordingly, it was found that the CNR of simulated hyperattenuating lesions can be substantially increased by using an 80-kVp, high tube current CT technique.

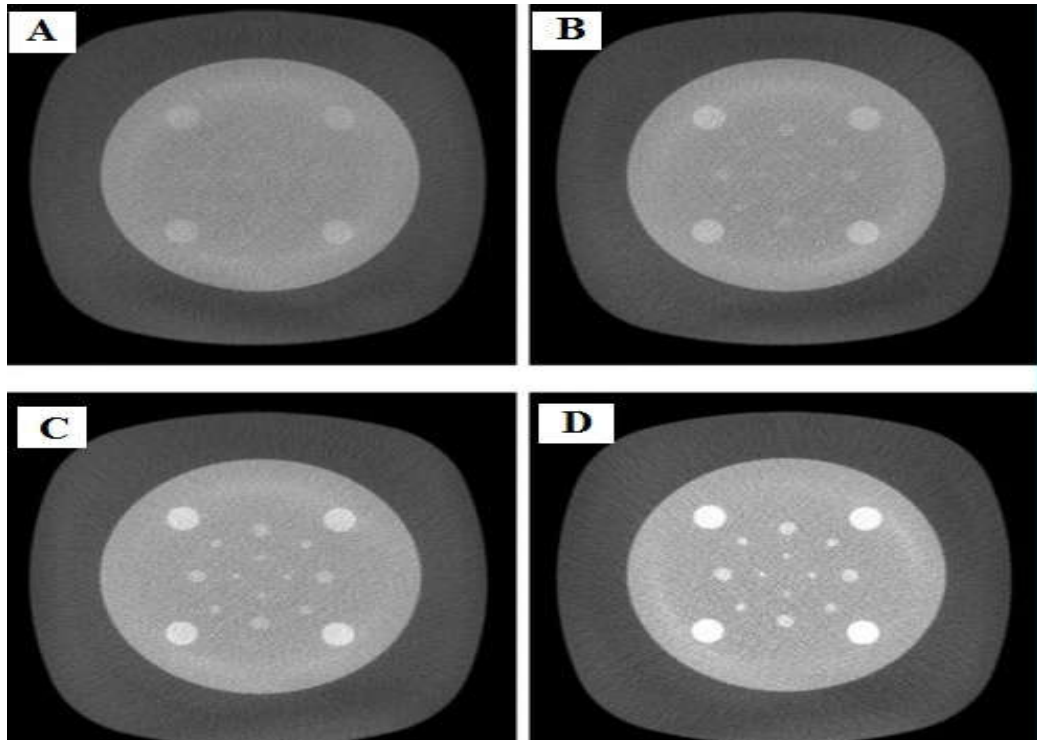


Figure 2.4 Four Axial CT images of liver phantom obtained with A) (140 kVp and 225 mAs), B) (120 kVp and 275 mAs), C) (100 kVp and 420 mAs), and D) (80 kVp and 675 mAs) protocols. On A, only four lesions were detected by the three radiologists, whereas on D, all lesions can be clearly delineated (Marin. et al., 2009b)

Yao et al. (2016) used a phantom and patients to evaluate the effect of SECT and DECT protocols on the CT image quality. Numerical anthropomorphic phantoms to mimic realistic clinical CT scans for medium and large size patients are used to simulate various SECT and DECT protocols at pre and post-contrast stages. For SECT, images from 60 kVp through 140 with 10 kVp steps are considered. As for DECT, both 80/140 and 100/140 kVp scans are simulated. To make a fair comparison, the mAs of each scan is adjusted to achieve the standard and the volume CT dose index ($CTDI_{vol}$) equivalent to standard protocols (120 kVp, 200 mAs for a medium-size patient and 140 kVp, 400 mAs for a large-size patient). CNR of the liver against other soft tissues is used to compare between the SECT and DECT protocols. Moreover, the authors conducted a clinical study, which included 166

patients. Eighty-five 120 kVp images and 81 blended 80/140 kVp images are compared via a quantitative image quality analysis and an observer study. In the phantom study, the authors found that the CNR of pre-contrast SECT image has generally increased with increasing kVp. However, for post-contrast imaging 90 kVp or lower, the results yielded higher CNR images. Similar trends are seen in DECT blended CNR and those from SECT protocols. In the presence of a differential iodine concentration (post-contrast), the CNR curves maximize at lower kVps (80–120). The combined pre and post-contrast composite CNR study demonstrated that an optimal SECT protocol achieved better performance than blended DECT images, and the optimal tube potential for SECT scan is around 90 kVp for medium-size patients and between 90 and 120 kVp for large-size patients (Yao et al., 2016).

Another study was conducted in 2017 to evaluate the simulated low contrast liver lesion detection in medium and large-size phantoms. The phantoms with 45 lesions are scanned at 70, 80, 100, and 120 kVp and the lesion-to-background CNR is calculated. The 120-kVp protocol served as a reference, and the $CTDI_{vol}$ was kept constant for all protocols ($CTDI_{vol}$, 8 mGray for the medium phantom and 19 mGray for the large phantom). The results confirmed that the lower tube voltages enhanced the detection of the liver lesions by increasing their CNR by 58%, 46%, and 16% at 70, 80, and 100 kVp, respectively compared with 120 kVp in the medium-patient size and by 9%, 18% and 12% in the large-patient size (Clark & Gunn, 2017).

Hokamp et al. (2018) evaluated the use of the virtual monoenergetic reconstruction technique to assess the hyperattenuating liver lesions in a phantom and patients (20 patients with 51 liver lesions). Images of the phantom with a lesion-mimicking are inserted and arterial phase images from contrast-enhanced patient

examinations are investigated at energy range 40–200 keV. CNR, signal to noise, and lesion to liver contrast are calculated at the regions of interest. The phantom results showed that the reconstructed images at 40 keV enhanced the assessment of the arterially hyperattenuating liver lesions because they increased the lesion contrast. In patients, the attenuation and lesion delineation were found to be the best in the low energy reconstructed image (40 keV), which also achieved the lowest perceptible noise and the best overall image quality (Hokamp et al., 2018).

2.1.1.3 Challenges in Liver Lesions Diagnosis via CT Examinations

The body contains objects and tissues with a variety of physical contrast and densities such as the ones that have a high physical contrast compared with the soft tissues. The imaging of high contrast regions, which have a big difference in CT numbers and densities, is not a challenging issue. The real challenge is the imaging of low-density areas, which have very low CT number differences among the tissues. If the contrast is low either because of the adjustments of the CT imaging protocol parameters or limitations of the specific imaging modality, then the tissues or pathologies that have small variations in physical contrast and density will not be visible (Lamba et al., 2014).

The lesions in liver are generally identified by a CT number difference between the lesion and the liver tissue. According to their small size and similar contrast to the surrounding liver tissue, liver lesions are difficult to be detected. The main problem of low contrast liver lesion detection from CT images is related to the low difference between CT numbers of the liver lesion and the liver tissue. The similarity in the CT number makes the detection of the lesions more difficult (Euler et al., 2017; Marin. et al., 2009b; Pooler et al., 2017; Schindera et al., 2011).

Although the iodine contrast improved liver lesions' visibility, the contrast-enhanced CT is still considered to be relatively insensitive in the depiction of small liver lesions. The small liver lesions are not often enhanced in post-contrast CT examinations because of a poor arterial blood supply and, therefore, they make them less conspicuous. These lesions are frequently mistaken as they typically show rapid homogeneous uptake of the iodine contrast with a rapid return to near-normal enhancement. They do not usually show high contrast enhancement (Abraham-Nordling et al., 2017; Marin. et al., 2009b; Tsuboyama et al., 2010; Valls et al., 2004).

Several studies showed that the low contrast small liver lesions (less than 2 cm) like focal nodular hyperplasia and hepatocellular carcinoma are not often detectable as large lesions in CT liver examinations (Abraham-Nordling et al., 2017; Brancatelli et al., 2001; Monzawa et al., 2007; Pazgan-Simon et al., 2015). These studies showed the poor quality of the CT image to attain early diagnosis of small-size liver lesions. However, early diagnosis of liver lesions is important to increase the possibility for curative surgery and, consequently, long-term survival (Lim et al., 2002; Quan et al., 2012; Tan et al., 2011). Therefore, further studies are required to enhance the diagnosis of low contrast small liver lesions in CT liver examinations.

2.2 Medical Physics Phantoms

A phantom is a specially designed object that mimics the human body in medical imaging examinations. The effects of radiation have become apparent with the early implementation of medical radiation. Therefore, people are reluctant to volunteer for experimental reasons. Consequently, physicists have developed phantoms to make

dosimetric measurements and to increase the quality of the image (Yohannes et al., 2012).

The properties of these materials differ with the energy of the radiation incident upon them. As a result, a phantom that is designed for kilovoltage beam will often be made from different materials than a phantom, which is designed for use in megavoltage X-ray beam. In order to give flexibility in imaging examinations and provide accurate knowledge of tissues' deformities, essential requirements are needed for manufacturing phantom materials including mass density, attenuation properties, and Z_{eff} value (DeWerd & Kissick, 2014; Hall et al., 1997). Furthermore, the chemical composition of the phantom materials should match the chemical composition of the simulated tissue. Therefore, the chemical composition of tissue-equivalent materials should mainly contain oxygen and carbon to match the composition of the human soft tissue (Claude et al., 2013; DeWerd & Kissick, 2014). Table 2.3 illustrates the elemental compositions, mass density, and Z_{eff} of body organ soft tissues (brain, kidney, and liver tissues) and common tissue-equivalent phantom materials.